ISSN- 2230-7346
Journal of Global Trends in Pharmaceutical Sciences

FORMULATION AND CHARACTERIZATION OF TRANSFEROSOMAL GEL LOADED WITH CLOTRIMAZOLE

G. Deepiga, C.P Sreekanth, J. Praveen Kumar, N. Audinarayana, D. Jothieswari

Sri Venkateswara College of Pharmacy (Autonomous), Chittoor, Andhra Pradesh, India

***Corresponding author E- mail: deepigaguru@gmail.com**

ARTICLE INFO

Key words:
vesicular, transferosomes, clotrimazole, transdermal.

Access this article online
Website:
https://www.jgtps.com/
Quick Response Code:

ABSTRACT

Clotrimazole, a broad-spectrum antifungal agent, suffers from a short biological half-life (~4 hours), necessitating frequent dosing to maintain therapeutic efficacy. To overcome this limitation and enhance localized delivery, the present study focused on the formulation and evaluation of a transferosomal gel system for sustained release and targeted cutaneous delivery of Clotrimazole. Drug-excipient compatibility was confirmed via Fourier Transform Infrared (FT-IR) spectroscopy, revealing no significant interactions. Preformulation studies included UV-spectrophotometric quantification of Clotrimazole at λ_max 271.5 nm in aqueous medium, demonstrating satisfactory reproducibility and precision.Transferosomal vesicles were developed using the thin film hydration technique, employing soya lecithin as the lipid component and ethanol as the permeation enhancer. The formulations were characterized for vesicle size (ranging from 368 to 931 nm), zeta potential, morphology (via microscopy), entrapment efficiency (65.45%–80.11%), solubility profile, and in vitro drug release kinetics. The optimized gel formulation exhibited a cumulative drug release of 79.90% over 24 hours.Kinetic modeling of the in vitro release data revealed a superior linear correlation (R^2) with the zero-order kinetic model compared to the first-order model, suggesting a concentration-independent, sustained release profile. The developed Clotrimazole-loaded transferosomal gel holds promise as an effective topical antifungal delivery system with enhanced residence time and controlled drug release.

INTRODUCTION

Conventional drug delivery modalities such as tablets, capsules, ointments, and injectables have long been employed to manage acute and chronic diseases. These systems typically provide immediate or rapid drug release, necessitating multiple daily administrations to sustain therapeutic plasma concentrations. Such regimens often lead to significant fluctuations in drug levels, which can compromise therapeutic efficacy and provoke adverse effects—particularly problematic in drugs with narrow therapeutic windows.To address these limitations, novel drug delivery systems (NDDS) have emerged, emphasizing controlled and sustained drug release. Among these, transdermal drug delivery systems (TDDS) have gained considerable traction due to their capacity to deliver drugs across the skin barrier either for localized or systemic therapeutic effects. TDDS bypass the hepatic first-pass effect and gastrointestinal factors such as pH variability, food-drug interactions, and enzymatic degradation, thereby enhancing systemic bioavailability and patient adherence. They are especially advantageous for patients who are noncompliant, unconscious, or suffering from nausea or dysphagia.Despite their promise, TDDS face notable limitations. The stratum corneum, the outermost layer of the epidermis, presents a formidable barrier to drug permeation due to its dense lipid matrix and low hydration. Only drugs with specific physicochemical characteristics—typically low molecular weight, high potency, and balanced lipophilicity—are suitable for transdermal delivery. Additionally, the cost of development, potential for skin irritation, and risk of misuse (e.g., improper application of patches) further constrain

widespread adoption.One of the prevalent indications for dermal and transdermal therapy is the treatment of fungal infections, which afflict approximately 1–2% of the global population. These infections, caused by pathogenic and opportunistic fungi such as *Candida*, *Aspergillus*, *Cryptococcus*, and *Histoplasma*, range from superficial cutaneous mycoses (e.g., tinea corporis, athlete's foot) to life-threatening systemic infections, particularly in immunocompromised individuals.Candida albicans, a polymorphic yeast, is a prominent cause of both mucocutaneous and invasive fungal infections. While it commonly colonizes mucosal surfaces and skin asymptomatically, disruptions in host immunity or skin integrity can lead to pathological overgrowth. Superficial candidiasis may manifest in intertriginous zones (e.g., axillae, groin) as erythematous rashes with satellite pustules. In contrast, invasive candidiasis may involve the bloodstream, lungs, liver, or other internal organs, often requiring aggressive systemic antifungal therapy.Given the skin's inherent barrier properties, enhancing dermal and transdermal drug permeation remains a significant challenge. To this end, vesicular drug delivery systemsincluding liposomes, niosomes, ethosomes, and transfersomeshave been developed. These nanocarriers encapsulate drugs to improve their solubility, stability, and permeation across biological membranes.Among these, **transfersomes** represent a superior class of ultra-deformable vesicles specifically designed for efficient transdermal delivery. First developed by Cevc and Blume, transfersomes are composed of phospholipids and edge activatorssurfactants such as sodium cholate or Tween 80—which destabilize the lipid bilayer to impart elasticity. This deformability enables them to traverse skin pores significantly smaller than their own diameter, propelled by the transdermal osmotic gradient between the relatively dry stratum corneum and the hydrated viable epidermis.Transfersomes follow two primary pathways through the stratum corneum: the intercluster route between corneocyte clusters and the intercorneocyte route between adjacent corneocytes. Their penetration is further enhanced by surface hydrophilicity and the synergistic action of ethanol and surfactants. Unlike conventional liposomes that are typically confined to the skin surface, transfersomes can deliver both low and high molecular weight therapeutics to deeper skin layers or systemic circulation.The standard method for transfersome preparation involves the thin-film hydration technique, where lipid components are dissolved in organic solvents, evaporated to form a thin film, hydrated with an aqueous buffer, and subsequently sonicated or extruded to produce nanometer-scale vesicles. These vesicles demonstrate high entrapment efficiency (up to 90% for lipophilic drugs), protect drugs from environmental degradation, and allow for sustained drug release. Furthermore, they are biocompatible, biodegradable, and amenable to large-scale production.Despite these advantages, transfersomal systems are not without challenges. Issues such as chemical instability, variability in the purity of natural phospholipids, high production costs, and sensitivity to oxidative degradation must be addressed for clinical translation.The current investigation aims to develop a **stable transfersomal gel formulation of Clotrimazole,** a broad-spectrum imidazole antifungal agent, for enhanced topical and transdermal delivery. The formulation seeks to overcome the skin's barrier function, enhance drug deposition in deeper layers, bypass first-pass metabolism, and provide **sustained antifungal activity** under non-occlusive conditions. Specific goals include optimizing vesicle deformability, maximizing drug entrapment, and evaluating skin permeation and therapeutic efficacy.

2. Material used: Clotrimazole, span 80, tween 80, Soya phosphatidylcholine , Methanol, Carbopol 934, Propylene glycol, Methyl Paraben Propyl Paraben.

3. Methodology: The transfersomal gel containing Clotrimazole was prepared using the thin film hydration technique. Initially, Soya phosphatidylcholine, span 80, Tween 80, and Clotrimazole were accurately weighed and dissolved in a solvent mixture of methanol (and optionally chloroform) in a round-bottom flask. The solvent was evaporated under reduced pressure using a rotary evaporator at 40°C to form a thin lipid film on the inner walls of the flask. The film was then kept in a vacuum desiccator overnight to remove any residual solvent. This dry film was hydrated with phosphate buffer (pH 7.4) preheated to 37°C and gently swirled to form transfersomal vesicles, followed by sonication to reduce vesicle size and ensure uniformity. Separately, a gel base was prepared by dispersing Carbopol 934 in distilled water and allowing it to swell. To this, propylene glycol, methyl paraben, and propyl paraben were added with continuous stirring. The pH of the gel

base was adjusted to approximately 6.0 using triethanolamine. Finally, the transfersomal suspension was incorporated into the gel base with gentle stirring to obtain a homogeneous Clotrimazole-loaded transfersomal gel, which was then stored in airtight containers at optimized temperature. The formulations developed with varied concentrations of Lecithin, Span 80, and Tween 80 are mentioned in the table 1 for reference.

3.1 Calibration curve: A stock solution was meticulously prepared by dissolving 20 mg of pure Clotrimazole in methanol and diluting it to 100 ml in a volumetric flask. Building upon this, a series of standard solutions with concentrations of 40 µg/ml, 60 µg/ml, 80 µg/ml, and 100 µg/ml were precisely formulated using methanol in separate volumetric flasks. Each solution was then subjected to UV spectrophotometer analysis at 272 nm (Table 2), with methanol serving as the reagent blank. This calibration curve formed the foundation for accurate and reliable quantification of Clotrimazole in subsequent formulations.

4. Evaluation studies:

4.1. Scanning Electron Microscopy (SEM): or Scanning Electron Microscopy (SEM) analysis, a small drop of the transferosome suspension was carefully placed on a clean glass coverslip mounted on an aluminum stub. The sample was then air-dried and sputter-coated with a thin layer of gold to render it conductive and prevent charging under the electron beam. The prepared specimen was observed under a scanning electron microscope at an accelerating voltage of 20 kV. High-resolution photomicrographs were captured at suitable magnifications, revealing detailed surface morphology, size, and shape of the transferosomes. This analysis provided critical insights into the structural integrity and uniformity of the vesicles, confirming their suitability for efficient drug delivery.

4.2. Particle size: The particle size of the transferosomes was determined using a dynamic light scattering (DLS) technique with a Zetasizer 300HS (Malvern Instruments, UK), a highly sensitive instrument designed for measuring nanoscale particle size and distribution. Prior to measurement, the transferosomal suspension was appropriately diluted with distilled water to avoid multiple scattering effects and ensure accurate results. The analysis was conducted at a controlled temperature of 25°C. The instrument calculates the hydrodynamic diameter based on the Brownian motion of particles, utilizing the autocorrelation function of the intensity of light scattered by the particles when irradiated with a laser beam. This method provides not only the average particle size but also the polydispersity index (PDI), which reflects the uniformity of the vesicle population. A lower PDI indicates a more homogeneous size distribution, which is critical for consistent drug release and stability of the formulation. The precise measurement of vesicle size plays a vital role in optimizing the performance of transferosomes as an efficient drug delivery system, influencing parameters like skin permeation and biodistribution.

4.3. Drug content: The drug content uniformity of the transferosomal formulation was evaluated in triplicate to ensure consistency and reliability. A known quantity of the transferosomal gel was accurately weighed and dissolved in methanol to extract the encapsulated drug. The resulting solution was subjected to centrifugation at 3000 rpm for 2 hours to separate any undissolved particles or lipid debris. The supernatant was then carefully collected and filtered through a 0.45 µm Whatman filter paper (Whatman, Maidstone, UK) to obtain a clear solution suitable for analysis. This filtrate was further diluted with methanol to bring the drug concentration within the linear range of Beer's Law. The absorbance of the final solution was measured using a UV-Visible spectrophotometer at the predetermined λmax of 272 nm, specific for Clotrimazole. The concentration of the drug was calculated from a previously established calibration curve. This method ensures accurate quantification of the active pharmaceutical ingredient and confirms the uniform distribution of the drug within the transferosomal formulation, which is critical for therapeutic efficacy and dose consistency.

4.4. EntrapmentEfficiency: The concentration of Clotrimazole in the transferosomal formulation was determined using UV spectrophotometric analysis after disrupting the vesicles with Triton X-100 (0.5% w/w), a non-ionic surfactant that effectively lyses lipid bilayers. The mixture of vesicles and Triton X-100 was centrifuged at 10,000 rpm for 10 minutes at 4°C to ensure complete separation of the lipid debris from the released drug. The supernatant was then carefully collected and filtered through a 0.45 µm membrane filter to obtain a clear solution. This filtrate was analyzed at 272 nm using a UV-Visible spectrophotometer, and the drug concentration was determined based on a previously

constructed calibration curve. From the absorbance data, the **entrapment efficiency (EE%),** which indicates the proportion of drug encapsulated within the vesicles, and the **drug loading efficiency(DL%),** which reflects the amount of drug per unit weight of the formulation, were calculated. These parameters are essential for evaluating the effectiveness, stability, and therapeutic potential of the transferosomal drug delivery system.

4.5.In vitro drug release studies: The in vitro permeation behavior of Clotrimazole from all transferosomal gel formulations, along with a control gel containing Clotrimazole, Span 80, Tween 80, and Soya phosphatidylcholine, was evaluated using a cellophane membrane with a molecular weight cut-off of 12,000–14,000 Da. A vertical Franz diffusion cell was specifically designed, fabricated, and validated for the study. The membrane was securely mounted between the donor and receptor compartments, with an effective diffusion area of 2.303 cm^2. The receptor compartment was filled with 22.5 mL of phosphate buffer (pH 7.4), maintained at 37 ± 0.5°C, and stirred continuously at 100 rpm to simulate physiological conditions. The prepared gel formulation was evenly applied to the membrane in the donor compartment. At predetermined time intervals, 2 mL aliquots were withdrawn from the receptor medium and replaced immediately with an equal volume of fresh buffer to maintain sink conditions. The cumulative amount of Clotrimazole permeated through the membrane was calculated and plotted as a function of time to assess permeation efficiency.

4.6.Kinetics of drug release: To determine the kinetic parameters of Clotrimazole release from the transferosomal gel formulations, the cumulative permeation data obtained from the in vitro diffusion study were analyzed using various mathematical models. The amount of drug permeated per unit area at each time point was calculated and plotted against time. The data were then fitted into different kinetic models, including Zero-order (cumulative drug release vs. time), First-order (log cumulative drug remaining vs. time), Higuchi model (cumulative drug release vs. square root of time), and the Korsmeyer-Peppas model (log of fractional drug release vs. log time). Each model was applied to determine the mechanism of drug release from the formulation. The correlation coefficient (R^2) was calculated for each model using regression analysis, and the model with the highest R^2 value was considered the best fit. This analysis helped identify whether the drug release was governed by diffusion, erosion, or a combination of mechanisms, thereby providing valuable insight into the release behavior and performance of the transferosomal gel.

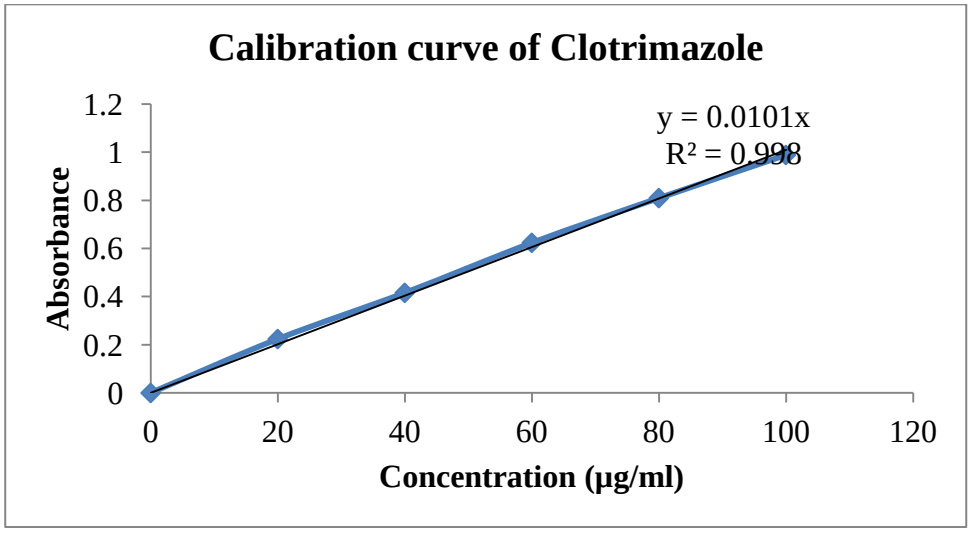

Figure 1: Calibration curve of clotrimazole

Table 1: Formulation chart representing the formulation details of Clotrimazole transferosomes

Formulation Code	Drug Mg	Lecithin mg	Span80 mg	Tween80 Mg	Methanol (ml)	Phosphate buffer(ml)

F1	10	95	5	-	2	10
F2	10	90	10	-	2	10
F3	10	85	15	-	2	10
F4	10	80	20	-	2	10
F5	10	75	25	-	2	10
F6	10	70	30	-	2	10
F7	10	95	-	5	2	10
F8	10	90	-	10	2	10
F9	10	85	-	15	2	10
F10	10	80	-	20	2	10
F11	10	75	-	25	2	10
F12	10	70	-	30	2	10

Table 2:Calibration curve data for Clotrimazole observed at 272 nm

S.No	Concentration (µg/ml)	Absorbance
1.	0	0
2.	20	0.214
3.	40	0.418
4.	60	0.596
5.	80	0.760
6.	100	0.931

5. RESULTS AND DISCUSSION: A successful attempt was made to formulate a transferosomal gel of Clotrimazole using various surfactants to study their impact on the properties of the formulations. A total of twelve different formulations were developed, with their compositions detailed in the corresponding table. The effect of the type and concentration of surfactants on the characteristics of the transferosomes was systematically evaluated. Among the prepared formulations, the most promising one, based on preliminary evaluations, was selected and incorporated into a Carbopol-based gel. Both the optimized transferosomes and the final gel formulation were subjected to comprehensive characterization to assess their physicochemical properties, ensuring their suitability for effective topical drug delivery.

5.1. DifferentialScanning Calorimetry (DSC Studies): The Differential Scanning Calorimetry (DSC) thermogram presented shows a clear endothermic peak occurring between approximately 170°C and 180°C, with an onset temperature of 173.07°C and a peak at 178.57°C. This peak is indicative of a melting transition, which is characteristic of a crystalline compound transitioning to its molten state. The enthalpy of fusion, represented by the area under the peak, is calculated to be 71.87 J/g, further supporting the presence of a distinct melting process. Following the melting endotherm, an exothermic peak is observed slightly above 180°C, which could correspond to recrystallization or decomposition depending on the nature of the sample. The sharpness of the melting peak and its relatively narrow temperature range suggest high purity and crystallinity of the compound. This thermogram provides valuable information about the thermal behavior of the sample, including its melting point, enthalpy of fusion, and possible post-melting events. However, The Differential Scanning Calorimetry (DSC) thermogram displayed above reveals a sharp endothermic peak with an onset temperature at 160.26°C and a peak maximum at 167.25°C. This well-defined endothermic event corresponds to the melting point of the sample, indicative of a crystalline phase undergoing a phase transition to a liquid.

The associated enthalpy of fusion is 115.3 J/g, suggesting a significant amount of energy is required for the melting process, which further supports the presence of a highly crystalline and possibly pure substance. The absence of additional thermal events before or after the melting peak implies thermal stability within the scanned range and no polymorphic transitions or decomposition events. Overall, this DSC thermogram provides crucial insight into the sample's thermal profile, particularly its melting behavior and purity.

5.2 Fourier Transform Infrared Spectroscopy (FTIR): The FTIR spectrum of Miconazole Nitrate reveals key functional groups present in the compound. A broad absorption around 3407 cm^{-1} corresponds to N–H stretching, indicating the presence of an imidazole ring. Peaks at 3177 and 3130 cm^{-1} represent aromatic C–H stretching, confirming aromatic structures. Aliphatic C–H stretches appear between 3029–3080 cm^{-1}, while a sharp peak at 1712 cm^{-1} suggests the presence of a carbonyl group, possibly from the nitrate component. Strong absorptions at 1588 and 1507 cm^{-1} correspond to C=C stretching in aromatic rings. Peaks near 1379 and 1274 cm^{-1} indicate nitro group vibrations, consistent with the nitrate salt. Finally, bands below 600 cm^{-1} suggest C–Cl or C–Br bonds, supporting the halogenated structure of miconazole.

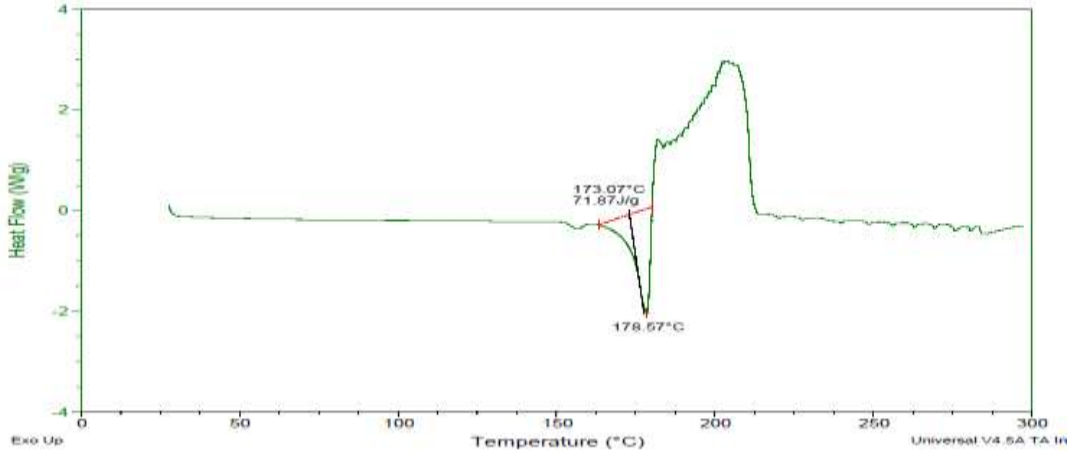

Figure 2: DSC graph of Clotrimazole

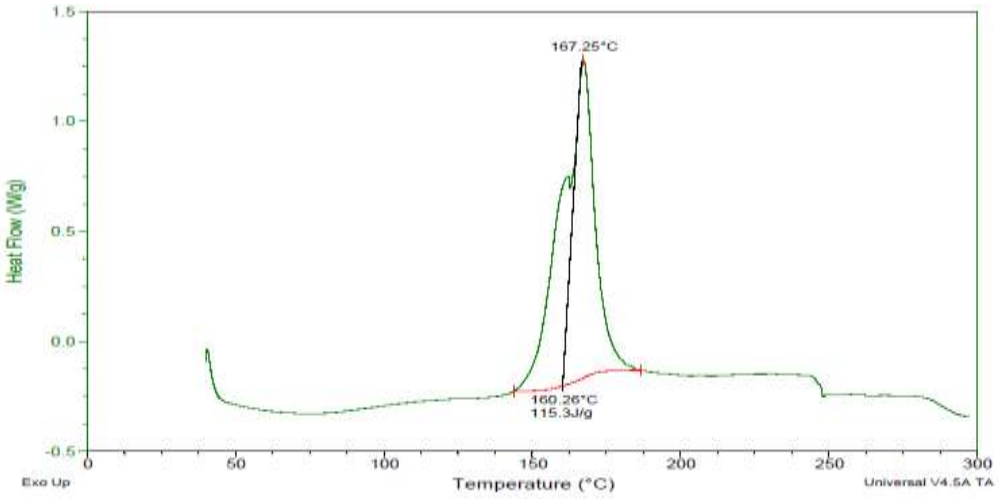

Figure 3: DSC graph of Clotrimazole along with the excipients

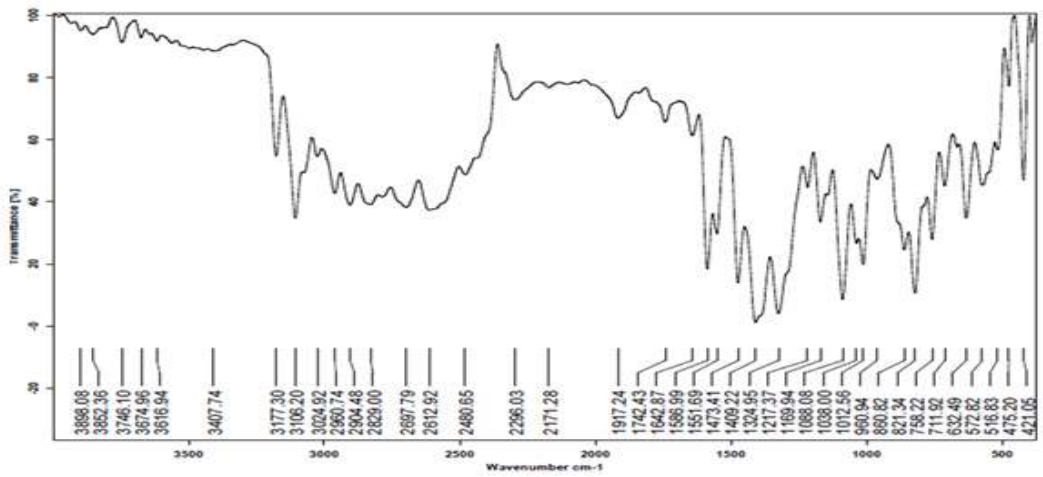

Figure 4:FTIR graph of Clotrimazole

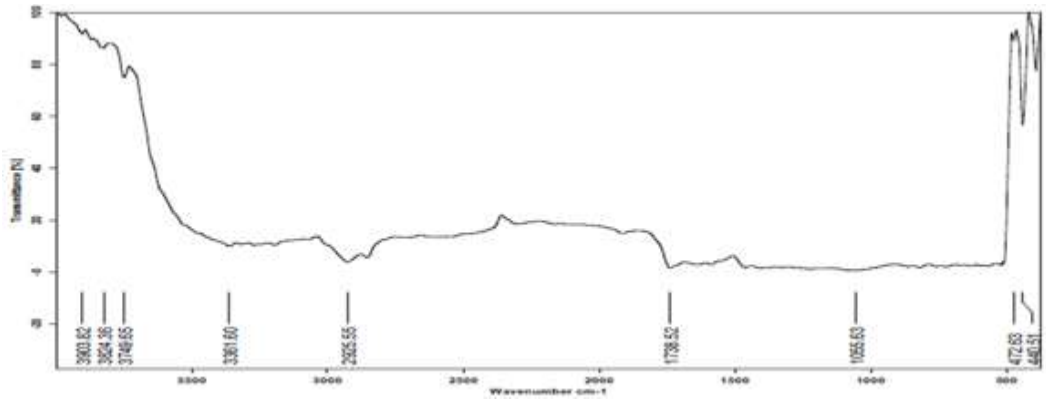

Figure 5: FTIR graph of Clotrimazole and Soyalecithin

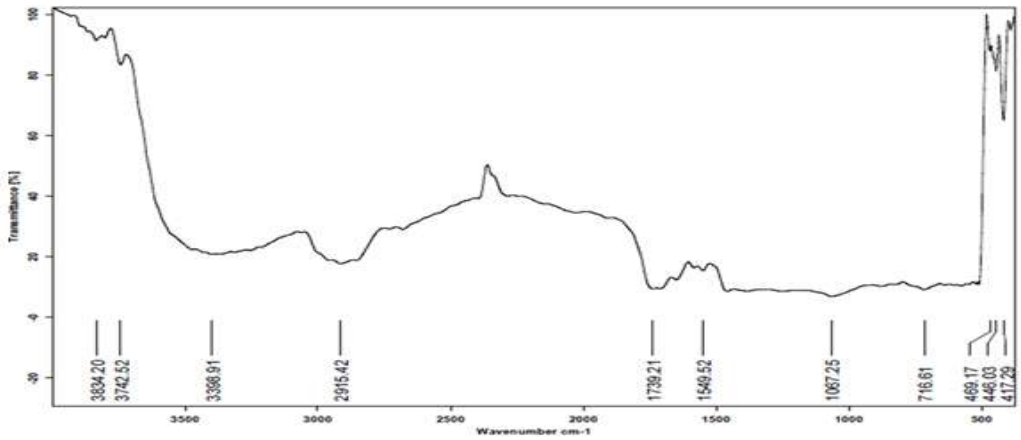

Figure 6: FTIR graph of Clotrimazole and Span 80

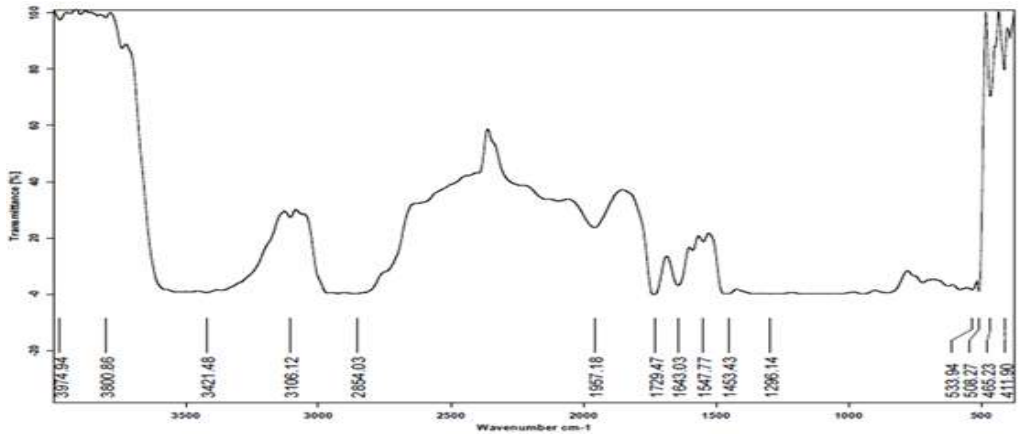

Figure 7: FTIR graph of Clotrimazole and Tween 80

Table 2: Summary of FTIR Interpretation

Functional group	Type of Vibration	Standard range	Observed range
Clotrimazole			
–OH or N–H (hydrogen bonding)	Stretching	3200–3600	3407.74
Aromatic C–H	Stretching	3000–3100	3177.30, 3130.20
Aliphatic C–H	Stretching	2850–3000	3080.92, 3029.40
C≡N or C≡C (nitrile/alkyne)	Stretching	2100–2260	2269.03
C=O (carbonyl group)	Stretching	1700–1750	1712.43
C=C (aromatic ring)	Stretching	1450–1600	1588.97, 1507.93
NO_2 (nitro group)	Asymmetric & Asymmetric bend	1300–1550	1379.47, 1274.23
C–O or C–N	Stretching	1000–1300	1170.93, 1088.06
Aromatic C–H out-of-plane bend	Bending	675–900	881.92, 822.24, 761.28
C–Cl or C–Br	Stretching	500–600	515.63, 475.30, 421.05

5.3 Scanning Electron Microscopy (SEM):
The prepared transferosomes were subjected to morphological evaluation using optical microscopy. A small quantity of the sample was carefully spread onto a clean glass slide and observed under an optical microscope. The visualization was carried out using a microscope integrated with Dewinter Microscopic Camera software, which enabled the capturing of high-resolution images of the vesicles. Morphological analysis revealed that the majority of the transferosomes exhibited spherical to oval shapes. The presence of oval-shaped vesicles may be attributed to slight deformation during sample preparation, possibly due to mechanical Stress or drying effects during slide preparation. Overall, the vesicles appeared to be well-formed, indicating the successful formulation of transferosomes suitable for further characterization and application.

5.4 Particle size and Drug content: Particle size analysis of the prepared transferosomal formulations revealed that the vesicle sizes ranged between 462 nm and 931 nm, classifying them within the nanometric scale and confirming the successful fabrication of nanosized carriers. The relatively small and consistent particle size is advantageous for enhanced skin penetration and stability of the formulation.Drug content uniformity was assessed in triplicate to ensure consistency and reproducibility of drug loading across formulations. For this analysis, a known

quantity of each formulation was accurately dissolved in methanol to disrupt the vesicular structure and release the encapsulated drug. The resulting solution was then subjected to centrifugation at 3000 rpm for 2 hours to eliminate any particulate matter or undissolved residues. The supernatant was subsequently filtered using a 0.45 µm Whatman filter paper (Whatman, Maidstone, UK) to obtain a clear solution.To quantify the drug content, the filtrate was appropriately diluted to fall within the linearity range of Beer-Lambert's law and analyzed using a UV-Visible spectrophotometer at the drug's maximum absorbance wavelength (λmax). The percentage drug content across the formulations was found to range from 80.45% to 94.15%, indicating efficient entrapment and uniform distribution of the drug within the transferosomal vesicles. These findings suggest that the method employed for transferosome preparation was effective in achieving high and consistent drug loading.

5.5 Entrapment Efficiency: The entrapment efficiency (EE%) of the prepared deformable vesicle formulations was evaluated to determine the capability of the transferosomes to encapsulate and retain the drug within their lipid bilayers. The EE% values were found to range from 66.12% to 80.11%, indicating a moderate to high efficiency of drug entrapment across the various formulations. This variability in entrapment efficiency can be attributed to the type and concentration of surfactants used, which influence the fluidity and packing of the lipid bilayer.Among the formulations containing Span 80 as the edge activator, formulation F3 demonstrated the highest entrapment efficiency of 80.11%, suggesting an optimal balance between vesicle deformability and drug encapsulation capability. In contrast, the lowest entrapment efficiency within the Span 80 group was observed in formulation F6, with a value of 65.41%, which may be due to suboptimal surfactant-to-lipid ratio or vesicle instability during formation.For the formulations containing Tween 80, the highest entrapment efficiency was recorded for formulation F10 at 74.25%, whereas formulation F8 showed the lowest EE% of 66.12% (Table 3). The comparatively lower entrapment efficiency in the Tween 80-based formulations could be due to the higher hydrophilicity of Tween 80, which may interfere with the hydrophobic interactions required for efficient drug encapsulation in the lipid bilayer.Overall, the results suggest that the type and concentration of surfactants significantly affect the entrapment efficiency of transferosomes. Span 80, being more lipophilic than Tween 80, tends to enhance drug entrapment in lipid bilayers, thereby contributing to higher EE% values. These findings are consistent with the observed particle size and drug content results, further confirming the influence of formulation variables on the physicochemical characteristics of transferosomal systems.

5.6 *In vitro* Diffusion Studies: The in vitro diffusion studies of all Clotrimazole-loaded transferosomal formulations were conducted using phosphate buffer (pH 7.4) to simulate physiological conditions. The release study was carried out over a 24-hour period, during which samples were withdrawn at predetermined intervals to calculate the cumulative percentage of drug released. The formulations were grouped as F1 to F6 and F7 to F12, and their respective drug release profiles were systematically tabulated and graphically represented by plotting cumulative drug release against time. These plots offered valuable insights into the release kinetics and performance of each formulation. A comparative evaluation revealed the significant influence of different types and concentrations of surfactants—namely Span 80 and Tween 80on the rate and extent of drug diffusion, highlighting the critical role of formulation composition in modulating drug release behavior.Furthermore, to assess the practical applicability of the system, in vitro release studies were also carried out using transferosomal gel formulations applied over a cellophane membrane. This model mimicked the drug release through a semi-permeable barrier, resembling topical application. The results were promising, with the optimized gel formulation achieving a maximum cumulative drug release of 88.62% within 24 hours. These findings underscore the potential of transferosomal gels as an efficient and sustained delivery platform for Clotrimazole, capable of maintaining prolonged therapeutic action with enhanced skin penetration.

In-vitro drug release Kinetics: The in vitro drug release data was meticulously analyzed using various kinetic models—Zero-order, First-order, Higuchi's, and the Korsmeyer-Peppas modelto unravel the mechanism and pattern of drug release from both Transferosomes and Transferosomal gel formulations.Upon fitting the

data to Zero-order and First-order kinetic models, a clear linear relationship emerged in both cases. However, the Zero-order model exhibited a significantly higher correlation coefficient (R^2), indicating that the formulations predominantly followed a Zero-order kinetic profile—characteristic of sustained and controlled drug This model, known for its precision in identifying drug release behavior, also showed excellent linearity with high R^2 values. The release exponent "n" for all formulations was found to be between 0.5 and 1.0, signifying that the drug release followed a non-Fickian or release.Further evaluation using Higuchi's model also demonstrated strong linearity, highlighting the role of diffusion as a contributing mechanism in the drug release process from the vesicular systems.To gain deeper insight into the exact release mechanism, the Korsmeyer-Peppas model was employed. anomalous diffusion mechanism—an interplay of both diffusion and erosion-controlled processes.Together, these findings paint a comprehensive picture of a well-orchestrated and sustained drug delivery system, offering valuable potential for advanced therapeutic application.

Table 3:Statistical data for particle size, drug content, and entrapment efficacy of prepared formulations

S.No	Formulation Code	Particle size (nm)	Drug content (%)	Entrapment efficiency (%)
1	F1	620	87.65	74.14
2	F2	741	81.43	69.42
3	F3	368	88.91	80.11
4	F4	721	90.31	71.78
5	F5	866	87.41	70.65
6	F6	871	94.15	65.41
7	F7	644	83.46	69.12
8	F8	702	80.45	66.12
9	F9	794	89.14	72.44
10	F10	462	85.16	74.25
11	F11	866	84.25	68.36
12	F12	931	88.16	72.11

Table 4: *In vitro* Diffusion Studies from F1-F6

S.No	Time (hr)	F1	F2	F3	F4	F5	F6
1	0	0	0	0	0	0	0
2	1	12.54	13.50	16.87	13.27	11.44	11.68
3	2	20.66	16.09	20.41	23.36	27.57	23.48
4	3	29.99	20.82	23.99	26.91	30.13	27.96
5	4	32.57	29.01	27.60	31.60	37.29	34.61
6	5	39.73	32.72	33.49	35.22	42.23	39.20
7	6	41.26	38.74	38.31	39.99	46.08	42.77
8	7	48.51	44.82	45.43	42.59	48.81	45.31
9	8	51.26	50.96	51.50	50.74	52.71	48.93
10	12	64.30	60.58	60.99	61.18	62.37	57.89
11	24	82.03	81.69	79.57	87.21	85.84	81.81

Table 5: *In vitro* Diffusion Studies from F7-F112

S.No	Time (hr)	F7	F8	F9	F10	F11	F12
1	0	0	0	0	0	0	0
2	1	16.77	19.88	15.70	21.13	13.05	19.28
3	2	31.32	28.78	20.35	24.87	17.93	24.01
4	3	32.83	34.04	27.28	28.64	25.23	28.78
5	4	37.94	39.35	32.03	33.61	30.23	35.87
6	5	41.91	42.22	40.20	42.16	32.90	44.16
7	6	48.31	50.09	45.08	46.10	39.15	49.13
8	7	51.17	53.06	47.76	47.72	47.84	53.01
9	8	60.05	63.51	51.59	54.05	51.86	56.93
10	12	71.41	74.07	62.18	65.13	63.05	65.41
11	24	87.67	88.45	82.97	83.37	79.08	88.72

Table 6:In-vitro drug release Kinetics from F1 to F6

S.No	Time (hr)	Log % Cumulative drug retained					
		F1	F2	F3	F4	F5	F6
1	0	2	2	2	2	2	2
2	1	1.941809	1.937016	1.919758	1.938169	1.947238	1.946059
3	2	1.899492	1.923814	1.900859	1.884455	1.859918	1.883775
4	3	1.84516	1.898615	1.880871	1.863858	1.844291	1.857574
5	4	1.828853	1.851197	1.859739	1.835056	1.797337	1.815511
6	5	1.780101	1.827886	1.822887	1.811441	1.761702	1.783904
7	6	1.768934	1.787177	1.790215	1.778224	1.73175	1.757624
8	7	1.711723	1.741782	1.736954	1.758988	1.709185	1.737908
9	8	1.687886	1.69055	1.685742	1.692494	1.674769	1.708166
10	12	1.552668	1.595717	1.591176	1.589056	1.575534	1.624385
11	24	1.254548	1.262688	1.310268	1.106871	1.151063	1.259833

Table 7:In-vitro drug release Kinetics from F7 to F12

S.No	Time (hr)	Log % Cumulative drug retained					
		F7	F8	F9	F10	F11	F12
1	0	2	2	2	2	2	2
2	1	1.92028	1.903741	1.925828	1.896912	1.93927	1.906981
3	2	1.83683	1.852602	1.901186	1.875813	1.914184	1.880756
4	3	1.827175	1.819281	1.861654	1.853455	1.873727	1.852602
5	4	1.792812	1.782831	1.832317	1.822103	1.843669	1.807061
6	5	1.764101	1.761778	1.776701	1.762228	1.826723	1.746945
7	6	1.713407	1.698188	1.739731	1.731589	1.784261	1.706462
8	7	1.688687	1.671543	1.718003	1.718336	1.717338	1.672005
9	8	1.601517	1.562174	1.684935	1.662286	1.682506	1.634175
10	12	1.456214	1.413803	1.577722	1.542452	1.567614	1.538951
11	24	1.090963	1.062582	1.231215	1.220892	1.320562	1.052309

Table 8: Higuchi model from F1 to F6

S. No	Square root of Time	% Cumulative drug release					
		F1	F2	F3	F4	F5	F6
1	0	0	0	0	0	0	0
2	1	12.54	13.50	16.87	13.27	11.44	11.68
3	1.414214	20.66	16.09	20.41	23.36	27.57	23.48
4	1.732051	29.99	20.82	23.99	26.91	30.13	27.96
5	2	32.57	29.01	27.60	31.60	37.29	34.61
6	2.236068	39.73	32.72	33.49	35.22	42.23	39.20
7	2.44949	41.26	38.74	38.31	39.99	46.08	42.77
8	2.645751	48.51	44.82	45.43	42.59	48.81	45.31
9	2.828427	51.26	50.96	51.50	50.74	52.71	48.93
10	3.464102	64.30	60.58	60.99	61.18	62.37	57.89
11	4.898979	82.03	81.69	79.57	87.21	85.84	81.81

Table 8: Higuchi model from F7 to F12

S.No	Square root of time	% Cumulative drug release					
		F7	F8	F9	F10	F11	F12
1	0	0	0	0	0	0	0
2	1	16.77	19.88	15.70	21.13	13.05	19.28
3	1.414214	31.32	28.78	20.35	24.87	17.93	24.01
4	1.732051	32.83	34.04	27.28	28.64	25.23	28.78
5	2	37.94	39.35	32.03	33.61	30.23	35.87
6	2.236068	41.91	42.22	40.20	42.16	32.90	44.16
7	2.44949	48.31	50.09	45.08	46.10	39.15	49.13
8	2.645751	51.17	53.06	47.76	47.72	47.84	53.01
9	2.828427	60.05	63.51	51.59	54.05	51.86	56.93
10	3.464102	71.41	74.07	62.18	65.13	63.05	65.41
11	4.898979	87.67	88.45	82.97	83.37	79.08	88.72

Table 9: Korsemeyer-Peppa'smodel from F1 to F6

S. No	Log Time	Log % Cumulative drug release					
		F1	F2	F3	F4	F5	F6
1	0	1.098298	1.130334	1.227115	1.122871	1.058426	1.067443
2	0.30103	1.31513	1.206556	1.309843	1.368473	1.440437	1.370698
3	0.477121	1.476976	1.318481	1.38003	1.429914	1.478999	1.446537
4	0.60206	1.512818	1.462548	1.440909	1.499687	1.571592	1.539202
5	0.69897	1.599119	1.514813	1.524915	1.546789	1.625621	1.593286
6	0.778151	1.615529	1.58816	1.583312	1.601951	1.663512	1.631139
7	0.845098	1.685831	1.651472	1.657343	1.629308	1.688509	1.656194
8	0.90309	1.709779	1.707229	1.711807	1.70535	1.721893	1.689575
9	1.079181	1.808211	1.782329	1.785259	1.786609	1.794976	1.762604
10	1.380211	1.913973	1.912169	1.900749	1.940566	1.93369	1.912806

Table 10: Korsemeyer-Peppa'smodel from F7 to F12

S.No	Log Time	Log % Cumulative drug release					
		F7	F8	F9	F10	F11	F12
1	0	1.224533	1.298416	1.1959	1.324899	1.115611	1.285107
2	0.30103	1.495822	1.459091	1.308564	1.395676	1.25358	1.380392
3	0.477121	1.516271	1.53199	1.435844	1.456973	1.401917	1.459091
4	0.60206	1.579097	1.594945	1.505557	1.526469	1.480438	1.554731
5	0.69897	1.622318	1.625518	1.604226	1.624901	1.517196	1.645029
6	0.778151	1.684037	1.699751	1.653984	1.663701	1.592732	1.691347
7	0.845098	1.709015	1.724767	1.679064	1.6787	1.679791	1.724358
8	0.90309	1.778513	1.802842	1.712566	1.732796	1.714833	1.755341
9	1.079181	1.853759	1.869642	1.793651	1.813781	1.799685	1.815644
10	1.380211	1.942851	1.946698	1.918921	1.92101	1.898067	1.948022

Table 11: *In-vitro* diffusion studies for transferosomal gel

S.No	Time (hr)	Abs (nm)	Con µg/ml	Con. mg/ml	Con. 100ml	Loss	CLS	CDR	%CDR
1	0	0	0	0	0	0	0	0	0
2	1	0.006	0.6	0.06	6	0	0	6	6.74
3	2	0.017	1.7	0.17	17	0.06	0.06	17.06	19.18
4	3	0.025	2.5	0.25	25	0.17	0.23	25.23	28.37
5	4	0.032	3.2	0.32	32	0.25	0.48	32.48	36.53
6	5	0.038	3.8	0.38	38	0.32	0.8	38.8	43.63
7	6	0.042	4.2	0.42	42	0.38	1.18	43.18	48.56
8	7	0.045	4.5	0.45	45	0.42	1.6	46.6	52.41
9	8	0.047	4.7	0.47	47	0.45	2.05	49.05	55.16
10	12	0.052	5.2	0.52	52	0.47	2.52	54.52	61.32
11	24	0.068	6.8	0.68	68	0.52	3.04	71.04	79.90

Table 12: *In-vitro*drug release kinetic data from F1 to F12

Formulation code	Zero order R^2	First order R^2	Higuchi's R^2	Korsemeyer Peppa's	
				n	R^2
F1	0.848	0.984	0.986	0.6	0.978
F2	0.886	0.991	0.977	0.633	0.969
F3	0.872	0.982	0.979	0.541	0.965
F4	0.91	0.993	0.992	0.594	0.988
F5	0.843	0.988	0.987	0.59	0.942
F6	0.862	0.987	0.993	0.585	0.969
F7	0.819	0.984	0.98	0.513	0.97
F8	0.806	0.978	0.974	0.495	0.982
F9	0.857	0.989	0.989	0.56	0.984
F10	0.842	0.978	0.988	0.473	0.973
F11	0.851	0.971	0.974	0.614	0.978
F12	0.844	0.992	0.987	0.518	0.978

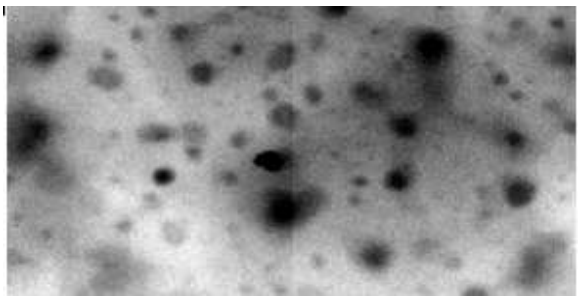

Figure 8: SEM of clotrimazole loaded transferosomes

CONCLUSION: Based on the findings of the study, it can be conclusively stated that the development of a Clotrimazole-loaded transferosomal gel presents a highly effective strategy for achieving sustained and targeted delivery of antifungal agents through the topical route. The formulation approach using soya lecithin and ethanol successfully yielded transferosomes with desirable physicochemical characteristics, including optimal particle size (368–931 nm), high entrapment efficiency (65.45%–80.11%), and stable zeta potential. The compatibility studies performed using FT-IR spectroscopy confirmed the absence of significant interactions between Clotrimazole and the selected excipients, indicating the chemical stability of the formulation components.The preformulation studies also established a reliable UV spectrophotometric method for drug quantification at λ_max 271.5 nm, which remained consistent throughout the research. The in vitro drug release studies demonstrated a prolonged release profile over 24 hours, with cumulative drug release ranging from 79.08% to 88.72%, and 79.90% specifically from the gel formulation. The release kinetics followed a zero-order model, indicating a controlled and concentration-independent drug release pattern, which is ideal for sustained therapeutic action.Overall, the transferosomal gel formulation enhances the pharmacokinetic profile of Clotrimazole by extending its half-life and maintaining therapeutic drug levels at the site of infection for a prolonged period. This system holds significant promise for improving treatment outcomes in fungal infections, reducing the frequency of application, and enhancing patient compliance, making it a potential candidate for future clinical development and commercial application.

REFERENCES:

1. Patel R, Singh S.K: Development and Characterization of Curcumin Loaded Transferosomes for Transdermal drug delivery. Int. J. Pharm. 2001, 71-80
2. Malakar J, Sen S, Nayak A and Sen K: Formulation, optimization and evaluation of Transferosomal gel for Transdermal insulin delivery. Saudi. Pharm.J. 2012, 437: 355–363.
3. Garg A, Negi A, Chauhan M: Gel Containing Ethosomal Vesicles For Transdermal Delivery Of Aceclofenac. Int. J. Pharm. Pharm. Sci. 2010, 2: 102-108
4. Patel RP, Patel GI, and Kamani R. Formulation, "Optimization and Evaluation of Mometasone Furoate Gel" Journal of Pharmacy Research, 2009; 2(11):720-724
5. Eldhose MP, Mathew F, Mathew NJ, "Transfersomes - A Review" International Journal of Pharmacy and Pharmaceutical Research, 2016; 6(4): 436-452.
6. Jivrani Shilpa D, Patel Vijay K, Formulation, "Development and Evaluation of Niosomal Drug Delivery System for Clindamycin Phosphate" Pharma Science Monitor, 2014; 5(2):256-274
7. Mishra M. and Biswal P, "Complexation, Optimization, Formulation development and characterization of clindamycin phosphate gel using zinc acetate dehydrate" International journal of pharmacy, 2012; 2(3):472-486
8. Rastogi V, Yadav P, "Transdermal drug delivery system: An overview" Asian

Journal of Pharmaceutics, 2012; 6(3):161-170. DOI:10.4103/0973-8398.104828

9. Mendonca CO, Burden AD, "Current concepts in psoriasis and its treatment" Pharmacology & Therapeutics, 2003; 99(2):133-147. https://doi.org/10.1016/S0163-7258(03)00041-X PMid:12888109
10. Schwartz, J.B., O'connor, R.E., Schnaare, R.L., 2007. Optimization technique in pharmaceutical formulation and processing. In: Banker, G.S., Rhodes, C.T. (Eds.), Modern Pharmaceutics, 4th edition. Marcel Dekker Inc, New York, pp. 607–627
11. Kumar, R., Philip, A., 2007. Modified transdermal technologies: Breaking the barriers of drug permeation via the skin. Trop. J. Pharm. Sci. 6, 633–644
12. Semalthy, A., Semalthy, M., Singh, R., Saraf, S.K., Saraf, S., 2007. Iontophoretic drug delivery system- a review. Technol. Health Care. 15, 237–245
13. Khafagy, E.S., Morishita, M., Onuki, Y., Takayama, K., 2007. Current challenges in non-invasive insulin delivery systems: a comparative review. Adv. Drug Deliv. Rev. 59, 1521–1546
14. Nayak, A.K., Laha, B., Sen, K.K., 2011. Development of hydroxyapatite-ciprofloxacin bone-implants using ''Quality by design''. Acta Pharm. 61, 25–36.
15. Yang, T.J., Wang, X.T., Yan, X.Y., Zhang, O., 2002. Phospholipids deformable vesicle for buccal delivery of insulin. Chem. Pharm. Bull. 50, 749–753.
16. Keyhanfar F, Shamsi Meymandi M, Sepehri G, Rastegaryanzadeh R, Heravi G. Evaluation of antinociceptive effect of pregabalin in mice and its combination with tramadol using tail flick test. Iran J Pharm Res. 2013;12(3):483
17. Mokhtar M, Sammour OA, Hammad MA, Megrab NA. Effect of some formulation parameters on flurbiprofen encapsulation and release rates of niosomes prepared from proniosomes. Int J Pharm. 2008;361(1–2): 104–111.
18. Xu X, Yu Z, Zhu Y, Wang B. Effect of sodium oleate adsorption on the colloidal stability and zeta potential of detonation synthesized diamond particles in aqueous solutions. Diam Relat Mater. 2005;14(2):206–212
19. Shaji J, Lal M. Preparation, optimization and evaluation of transferosomal formulation for enhanced transdermal delivery of a COX-2 inhibitor. Int J Pharm Pharm Sci. 2014;6(1):467–477.
20. Das MK, Maurya DP. Evaluation of Diltiazem hydrochlorie-loaded mucoadhesive microspheres prepared by emulsification-internal gelatin technique.ActaPoloniae Pharmaceutica and Drug Research.2008; 65(2):249-259.
21. Zhang, J. P., Wei, Y. H., Zhou, Y., Li, Y. Q. & Wu, X. A. Ethosomes, Binary Ethosomes and Transfersomes of Terbinafine Hydrochloride: A Comparative Study. Arch. Pharm. Res, 2012; 35 (1): 109– 117.
22. Cevc, G. Lipid vesicles and other colloids as drug carriers on the skin. Adv. Drug Deliv. Rev. 2004, 56, 675–711.
23. Walve, J.R.; Bakliwal, S.R.; Rane, B.R.; Pawar, S.P. Transfersomes: A surrogated carrier for transdermal drug delivery system. Int. J. Appl. Biol. Pharm. Technol. 2011, 2, 204–213.